Electrocatalysis (2018) 9:662–672
https://doi.org/10.1007/s12678-018-0474-2

ORIGINAL RESEARCH

A Combined DFT and Experimental Investigation of Pt-Wrapped CoNi Nanoparticles for the Oxygen Reduction Reaction

E. Flores-Rojas[1] · H. Cruz-Martínez[1] · H. Rojas-Chávez[2] · M. M. Tellez-Cruz[3] · J. L. Reyes-Rodríguez[3] · J. G. Cabañas-Moreno[1] · P. Calaminici[3] · O. Solorza-Feria[3]

Published online: 16 May 2018

Abstract

CoNi bimetallic nanoparticles wrapped with Pt were the subject of a theoretical study and experimental validation for the oxygen reduction reaction (ORR). The computational study was carried to evaluate the effect of the core composition of the Pt-wrapped CoNi nanoparticles toward the ORR. For this purpose, Pt_{44} and Co_nNi_{6-n}-Pt_{38} ($0 \le n \le 6$) octahedral nanoparticles were employed as models and the O and OH binding energies were taken into account to describe the ORR electrocatalytic activity. The experimental validation of these type of nanoparticles was performed considering two compositions ($Co_{30}Ni_{70}$-20Pt/C and $Co_{70}Ni_{30}$-20Pt/C). The Co_nNi_{6-n}-Pt_{38} ($0 \le n \le 6$) nanoparticles exhibit O and OH adsorption energies weaker than the pure Pt_{44} nanoparticles, suggesting, therefore, a higher electrocatalytic activity for the CoNi-Pt with respect to one of elemental Pt nanoparticles. The electrochemical results confirm the theoretical prediction, showing that the $Co_{30}Ni_{70}$-20Pt/C and $Co_{70}Ni_{30}$-20Pt/C electrocatalysts present higher specific activities, 400% and 300%, above that of Pt/C, respectively, as well as mass activities 50% higher than the commercial Pt/C, taken as reference.

Keywords ADFT · Reactivity · Electrocatalytic activity · High-energy milling · Galvanic displacement

Introduction

The prohibitive cost of noble metals and the sluggish kinetics of the oxygen reduction reaction (ORR) have been some of the major challenges for mass commercialization of the proton exchange membrane fuel cells (PEMFCs) [1–3]. Many research groups focus their attention on the development of new electrocatalysts for the ORR. Pt-based nanocatalysts are extensively investigated as substitutes to pure Pt catalysts due to their proven effectiveness in the ORR [4–11]. Alloy nanoparticles wrapped with Pt have gained special attention because they exhibit a good electrocatalytic activity for the ORR. Several studies were conducted to explore the implementation of bimetallic cores that contain a combination of noble and non-noble transition metals with a Pt monolayer as shell, leading to very promising materials [12–15]. Nonetheless, the use of noble metals, in both core and shell parts of the nanoparticle, results in high noble metal catalyst loading and, consequently, higher production costs. To address this, research efforts currently focus in the design of nanoparticles with cores formed by two non-noble metals to serve as a new generation of electrocatalysts for the ORR.

Electronic supplementary material The online version of this article (https://doi.org/10.1007/s12678-018-0474-2) contains supplementary material, which is available to authorized users.

✉ H. Cruz-Martínez
hcruzm@cinvestav.mx

✉ P. Calaminici
pcalamin@cinvestav.mx

✉ O. Solorza-Feria
osolorza@cinvestav.mx

[1] Programa de Doctorado en Nanociencias y Nanotecnología, CINVESTAV, Av. Instituto Politécnico Nacional 2508, San Pedro Zacatenco, Gustavo A. Madero, C.P. 07360 Ciudad de México, Mexico

[2] Departamento de Física, CINVESTAV, Av. Instituto Politécnico Nacional 2508, San Pedro Zacatenco, Gustavo A. Madero, C.P. 07360 Ciudad de México, Mexico

[3] Departamento de Química, CINVESTAV, Av. Instituto Politécnico Nacional 2508, San Pedro Zacatenco, Gustavo A. Madero,, C.P. 07360 Ciudad de México, Mexico

Two systems have been recently reported (Pt-wrapped Co and Ni nanoparticles) [16] whose catalytic activities are similar to that of Pt (Etek). In that work, it was theorized that the ORR electrocatalytic activity could improve without the use of noble metals in the cores, making the case for the use of a Ni and Co system for the core, and Pt as the shell of the nanoparticle. In a secondary study, a $Co_{50}Ni_{50}$ system wrapped with Pt (~20 wt.%) was reported [17]. The Pt-wrapped CoNi nanoparticles presented mass and specific activities higher than Pt (Etek). This work borrows from the results of the secondary study and implements modifications to the reported synthesis method in order to achieve greater Pt coverage of the bimetallic cores of the nanoparticles and to experimentally demonstrate that the CoNi bimetallic cores wrapped with Pt are more active than materials with monometallic cores [16, 17].

Through improvements of density functional theory (DFT), it is possible to predict catalytic activities of different nanoparticles [18]. In terms of the ORR, various investigations have been performed to correlate first-principles calculations and experimental results. In most studies, binding energies of adsorbates (O, OH, O_2) as well as the d-band center energy are used to describe the ORR electrocatalytic activity [19–21]. The catalytic descriptor values are directly related to the mass and specific activity experimentally obtained, and it has been proposed that the best catalysts should show an O adsorption energy roughly 0.2 eV weaker than pure Pt [19–21]. There are several theoretical works that discuss surface [22–24] and nanoparticle models [25–27] to propose new nanocatalysts for the ORR. Recently, several comprehensive studies with theoretical models and experimental validation for the design of M@Pt (M = Ni, Os, Co, Cu, Pd) and AuPd@Pt core–shell nanoparticles have been reported [28–32]. These studies could be a turning point in the design of better electrocatalysts for the ORR.

Based upon the excellent contributions of those works, this study addresses a theoretical and experimental approach for the development of CoNi bimetallic nanoparticles wrapped with Pt for the ORR in an acid medium. In a computational section, the effect of the core composition of the CoNi bimetallic nanoparticles wrapped with Pt toward the ORR is presented. For this purpose, Pt_{44} and Co_nNi_{6-n}-Pt_{38} ($0 \le n \le 6$) octahedral nanoparticles were used as models, while computed O and OH adsorption energies were used to describe the ORR electrocatalytic activity. We use the O and OH adsorption energies since the O and OH species have been shown to be the best descriptors for the catalytic activity toward the ORR. The experimental validation of the theoretical results of the CoNi bimetallic nanoparticles wrapped with Pt was performed by evaluating two compositions ($Co_{30}Ni_{70}$-20Pt/C and $Co_{70}Ni_{30}$-20Pt/C).

Materials and Methods

Computational Details

The computations were performed employing the deMon2k program which makes use of the auxiliary density functional theory (ADFT) [33, 34]. A fine grid was considered to integrate the exchange-correlation potential [35, 36]. The calculations of the Coulomb energy were performed by considering the variational fitting procedure proposed by Dunlap and collaborators [37, 38]. The PBE98–PBE96 functional was employed in all computations [39, 40]. The Pt atom was described with an 18-electron QECP|LANL2DZ basis set [41]. The Co, Ni, O, and H atoms were described with all-electron DZVP basis sets optimized for GGA functionals [42]. The GEN-A2* auxiliary function set was used [42]. The calculations were performed with the restricted open-shell Kohn–Sham (ROKS) methodology [43]. The geometry optimization was performed using a quasi-Newton optimization method in delocalized internal coordinates [44]. To investigate the potential energy surfaces of the studied systems, spin multiplicities from singlet up to 29 were investigated. The spin multiplicity (M) is calculated as M = 2S + 1, with S being the sum of the unpaired electrons in each system.

In this investigation, to evaluate the effect of the core composition of the CoNi bimetallic nanoparticles wrapped with Pt on the electrocatalytic activity for the ORR, octahedra-shaped nanoparticles of 44 atoms (containing 6 atoms in the core and 38 atoms in the shell) were modeled. The CoNi bimetallic nanoparticles wrapped with Pt are denoted as Co_nNi_{6-n}-Pt_{38} ($0 \le n \le 6$). The O and OH adsorption energies were calculated and used as descriptors of the electrocatalytic activity for the ORR. To calculate the species adsorption energies (O or OH) on the Co_nNi_{6-n}-Pt_{38} ($0 \le n \le 6$) and Pt_{44} nanoparticles, the O atom and OH molecule were adsorbed on each face of the octahedra nanoparticles (a total of eight species were adsorbed at the same time for each nanoparticle; see Fig. 3). The selected arrangements of the O and OH adsorbates taken in consideration in our study are the ones which in the literature are stated as the most investigated. Therefore, the O atoms were adsorbed on hollow sites whereas the OH molecules were adsorbed on top sites. The average O adsorption energies (E_{ads}) were calculated by averaging over the eight adsorption sites using protocols previously reported [26], The O E_{ads} was therefore calculated as follows:

$$E_{ads}(O) = \frac{1}{8}\left(E_{NP+8O} - E_{NP} - 8E_O\right) \quad (1)$$

where E_{NP+8O} is the energy of the nanoparticle with eight O atoms adsorbed, E_{NP} is the energy of the optimized nanoparticle, and E_O is the energy of the free oxygen atom.

The average OH adsorption energies ($E_{ads}(OH)$) were calculated by averaging over the eight adsorption sites as

$$E_{ads}(OH) = \frac{1}{8}(E_{NP+8OH} - E_{NP} - 8E_{OH}) \quad (2)$$

where E_{NP+8OH} is the energy of the nanoparticle with eight OH molecules adsorbed, E_{NP} is the energy of the optimized nanoparticle, and E_{OH} is the energy of the free OH molecule. The O and OH adsorption energies of the Co_nNi_{6-n}-Pt_{38} ($0 \le n \le 6$) nanoparticles with respect to the Pt_{44} nanoparticles were studied via the relative adsorption energy, defined as

$$E_{ads,rel} = E_{ads}(sys) - E_{ads}(Pt) \quad (3)$$

where $E_{ads,rel}$ is the relative O or OH adsorption energy of the Co_nNi_{6-n}-Pt_{38} ($0 \le n \le 6$) nanoparticles with respect to the pure Pt_{44} system, $E_{ads}(sys)$ is the adsorption energy of O or OH on the selected system, and $E_{ads}(Pt)$ is the adsorption energy of the O or OH on the pure Pt_{44} system, respectively.

Experimental Procedure

The experimental validation of the computed results of the CoNi bimetallic nanoparticles wrapped with Pt was performed by varying the composition of the CoNi bimetallic core ($Co_{30}Ni_{70}$-20Pt/C and $Co_{70}Ni_{30}$-20Pt/C). Details of the implemented experimental procedure are given in the following subsections.

High-Energy Milling

High-energy milling (HEM) has demonstrated to be a reproducible, scalable, and inexpensive technique for the synthesis of nanomaterials [45–48]. Nanoparticles of $Co_{30}Ni_{70}$ and $Co_{70}Ni_{30}$ (atomic ratio) combinations were produced by HEM of Co and Ni powders. A detailed description of this procedure is presented in our previous study [16].

Catalyst Dispersion on Carbon and Galvanic Displacement

To decorate the milled systems with platinum, the experimental procedure here described was modified with respect to a procedure previously reported in literature [16]. The three differences are as follows: (1) no need for dispersing agents; (2) use of an ultrasonic processor with long ultrasonic treatments; (3) the vortex mixer was replaced with the ultrasonic processor. Initially, milled powders were dispersed by sonication for 30 min with the aid of an ultrasonic processor, whereas carbon black (Vulcan XC-72R) was dispersed by sonication for 30 min in an ultrasonic bath. For dispersion, a mix of isopropyl alcohol (50% *v*/*v*) and ultrapure water (50% *v*/*v*) (Milli-Q, 18.2 MΩ cm resistivity) was used. Finally, each milled system was added to the carbon black solution, with a metal-to-carbon weight ratio of 1:1, and then the mixed powders–carbon were sonicated for 30 min to achieve dispersion on carbon black.

Galvanic displacement was used to decorate each milled system with Pt. A solution of K_2PtCl_6 salts was employed as the Pt precursor reagent. The solution of Pt salt was dripped into the powder–carbon and dispersing mixture under sonication (30 min). After a reflux process of 5 h, with magnetic stirring was carried out. Finally, the product was collected by centrifugation after being washed with deionized water and dried for 3 h at 110 °C in an argon atmosphere.

Physical and Electrochemical Characterization

The physical characterization was performed by employing X-ray diffraction (XRD), scanning transmission electron microscopy (STEM), inductively-coupled plasma mass spectrometry (ICP-MS), atomic absorption spectroscopy (AAS), and energy-dispersive X-ray spectroscopy (EDX-SEM). XRD was used for the phase identification of the two synthesized nanocatalysts. XRD patterns were measured in a Bruker D8 advance eco diffractometer using Cu Kα radiation (λ = 1.5418 Å) operating at 40 kV and 25 mA at room temperature. STEM was employed to determine the particle size and morphology of the two nanocatalysts and performed with an ARM200F-JEOL microscope operating at 200 keV. A Thermo Scientific iCE 3300 equipment was used to conduct AAS to obtain a quantitative chemical analysis of Co and Ni compositions; for platinum composition analysis, ICP-MS was performed with a Perkin Elmer Optima 8300 spectrometer. EDX-SEM was used for surface chemical analysis of the two electrocatalysts using a Bruker EDAX detector coupled to an Auriga Zeiss Scanning Electron Microscope (model 3916) operated at high vacuum.

Cyclic voltammetry (CV), CO stripping, and rotating disk electrode (RDE) measurements were used for the electrochemical evaluation. The electrochemical measurements were performed using a potentiostat/galvanostat (PARSTAT model 2273). Experiments were done in a conventional three-electrode electrochemical cell. A platinum mesh was employed as counterelectrode and a normal hydrogen electrode (NHE) as reference electrode. RDE measurements were performed on a thin film catalyst (30 μg cm^{-2}) deposited on the surface of a glassy-carbon disk electrode (0.196 cm^2). The quantitative chemical analysis measured by EDX-SEM and ICP-MS for the $Co_{30}Ni_{70}$-20Pt/C system revealed compositions close to the nominal composition, and EDX-SEM analysis of the $Co_{70}Ni_{30}$-20Pt/C system also revealed a composition similar to the nominal composition. For this reason, the Pt loadings had to be fitted (Table 1). Detailed descriptions for the CV, CO stripping and RDE electrochemical setup have been described in previous studies [17]. For CV measurement,

Table 1 Quantitative analyses performed by EDX-SEM and ICP-MS for the $Co_{30}Ni_{70}$-20Pt, and EDX-SEM for the $Co_{70}Ni_{30}$-20Pt

Systems	Nominal composition (Co–Ni–Pt)	EDX-SEM (Co–Ni–Pt)	ICP-MS (Co–Ni–Pt)
$Co_{30}Ni_{70}$-20Pt	24–56–20	10.4–64.6–25	8.6–68.8–22.6
$Co_{70}Ni_{30}$-20Pt	56–24–20	37–28.5–34.5	–

30 potential cycles at 50 mV s^{-1} between 0.05 and 1.20 V were carried out in a N_2-saturated 0.1 M $HClO_4$ solution until stable voltammetry curves were obtained. CO stripping measurements were obtained by saturating the work solution with CO for 300 s, followed by 600 s of N_2, and running electrochemical tests of 3 cycles at 20 mV s^{-1} between 0.05 and 1.20 V with an adsorption potential of 0.1 V. The ORR measurements were performed at 20 mV s^{-1} in O_2-saturated solution from 0.05 to 1.05 V. The ohmic drop in all measurements (15–25 Ω) was electronically compensated by the potentiostat by a positive feedback method. Three measurements for each experiment were carried out to demonstrate reproducibility.

Results and Discussion

Averaged Bond Lengths of Pt_{44} and Co_nNi_{6-n}-Pt_{38} ($0 \le n \le 6$) Octahedral Nanoparticles

The structures of the Pt_{44} and Co_nNi_{6-n}-Pt_{38} ($0 \le n \le 6$) octahedral nanoparticles employed in this study are presented in Fig. 1. Several factors can explain the higher electrocatalytic activity of the Pt-based alloys with respect to the pure Pt. One of them is compressive strain due to shorter Pt–Pt bond length caused by the non-noble metals to which they are alloyed [49, 50]. Figure 2 presents the average length for Pt–Pt bonds (Å) corresponding to platinum atoms located on the surface of the Pt_{44} and Co_nNi_{6-n}-Pt_{38} ($0 \le n \le 6$) octahedral nanoparticles. It was observed that the average Pt–Pt bond length calculated for the Co_nNi_{6-n}-Pt_{38} ($0 \le n \le 6$) octahedral nanoparticles decreases with respect to that of a pure Pt_{44} nanoparticle (Fig. 2). The decrease of the Pt–Pt bond length of the Co_nNi_{6-n}-Pt_{38} ($0 \le n \le 6$) nanoparticles with respect to Pt_{44} is in the range of 0.027–0.034 Å. This decrease can be attributed to the coordination of the Ni and Co atoms with the Pt atoms.

Reactivity Descriptors

Oxygen Adsorption Energies on the Pt_{44} and Co_nNi_{6-n}-Pt_{38} ($0 \le n \le 6$) Octahedral Nanoparticles

A descriptor commonly employed to evaluate the electrocatalytic activity of the nanocatalysts for ORR is the binding energy of the adsorbates. Sabatier's principle mentions that active nanocatalysts should have a well-defined, optimal adsorption energy value. If the adsorption is weak, the surface reaction of the adsorbed species would not occur, whereas if the adsorption is strong, this would lead to the poisoning of the surface-active sites of the nanocatalysts [26, 51]. The most used descriptor to predict the electrocatalytic activity of the ORR is the O binding energy. To compute the average oxygen adsorption energies, the O atom was adsorbed on eight different sites for each type

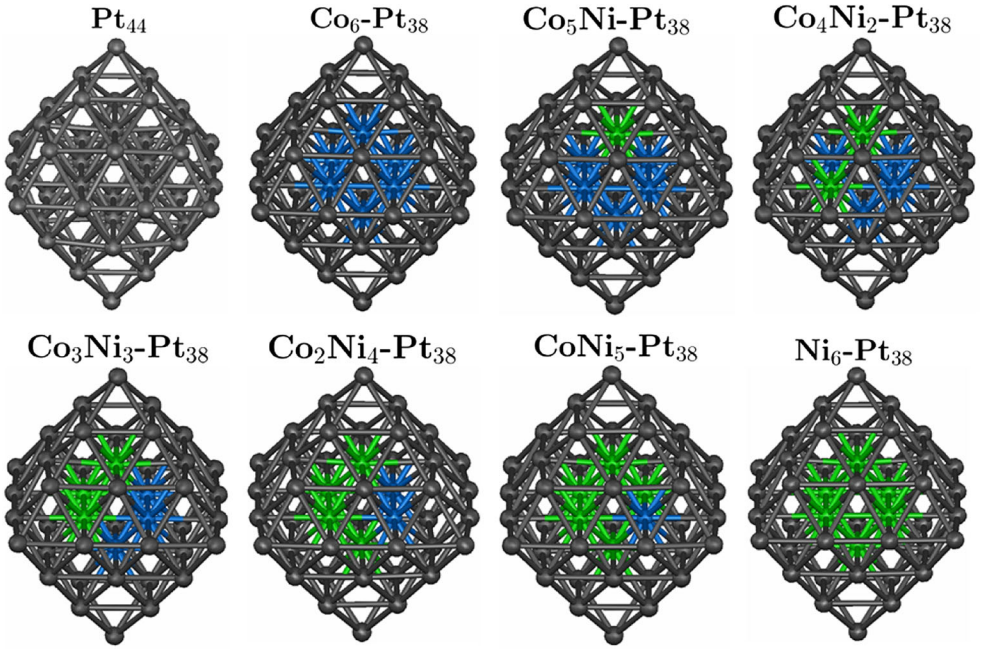

Fig. 1 Structures of the Pt_{44} and Co_nNi_{6-n}-Pt_{38} ($0 \le n \le 6$) octahedra nanoparticles. Black, blue, and green spheres represent Pt, Co, and Ni atoms, respectively

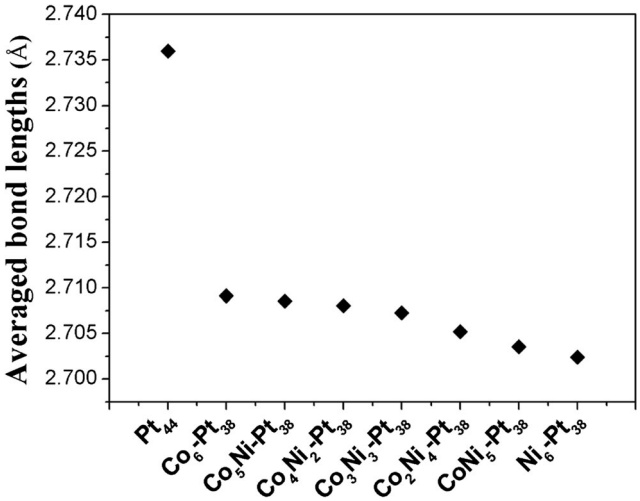

Fig. 2 Averaged Pt–Pt bond lengths (Å) of the Pt_{44} and Co_nNi_{6-n}-Pt_{38} (0≤n≤6) octahedral nanoparticles

of nanoparticle. In Fig. 3a, the eight sites of O adsorption on the Pt_{44} octahedron nanoparticle are illustrated (here, the Pt_{44} nanoparticle is used as an example to show the O adsorption sites on the nanoparticles presented in Fig. 1).

Figure 4a shows the relative oxygen adsorption energies of the Co_nNi_{6-n}-Pt_{38} (0≤n≤6) octahedral nanoparticles with respect to pure Pt_{44} nanoparticles. Nørskov and collaborators demonstrated that the best electrocatalysts should exhibit an oxygen adsorption energy which is roughly 0.2 eV weaker than pure Pt [19, 20]. The Ni_6-Pt_{38} and Co_6-Pt_{38} nanoparticles have an adsorption energy weaker than the Pt_{44} nanoparticle. These results are consistent with those reported in theoretically data, in which the M@Pt core–shell nanoparticles (M = 3d elements) present a lower O adsorption energy with respect to the one of pure platinum [26, 52, 53]. This has been experimentally corroborated and it has been shown that M-Pt bimetallic nanoparticles exhibit greater electrocatalytic activity than the one of pure platinum for the ORR [54, 55].

There are scarce theoretical studies on nanoparticles formed with 3d elements, bimetallic cores, and surrounded

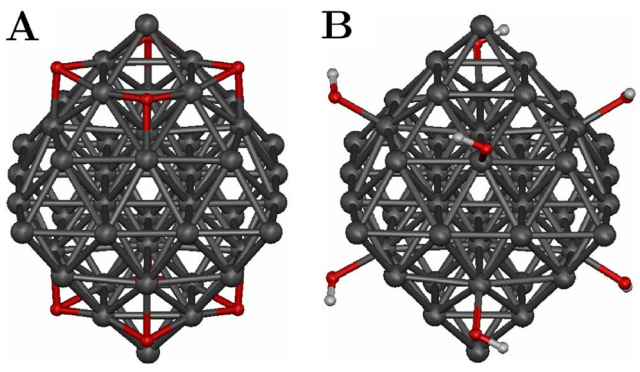

Fig. 3 Sites of O and OH adsorption on the Pt_{44} octahedron nanoparticle. **a** Sites of O adsorption on the Pt_{44} octahedron nanoparticle and **b** sites of OH adsorption on the Pt_{44} octahedron nanoparticle. Black, red, and gray spheres represent Pt, O, and H atoms, respectively

by platinum shells. Therefore, this work treats the composition of Co_nNi_{5-n} (1≤n≤5) bimetallic cores wrapped with Pt and compares the O adsorption energy of these nanoparticles to those of monometallic core structures (Ni_6-Pt_{38} and Co_6-Pt_{38}) and pure Pt_{44} nanoparticles. Figure 4a shows that the Co_nNi_{5-n}-Pt_{38} (1≤n≤5) nanoparticles present an adsorption energy (≈ 0.12–0.25) weaker than the one for pure Pt_{44} nanoparticles, making them good candidates for the ORR reaction. Therefore, by using O as a predictor of the catalytic activity, it is expected that the CoNi-Pt nanoparticles will have higher electrocatalytic activity than the Pt nanoparticles.

OH Adsorption Energies on the Pt_{44} and Pt_{38}-Wrapped Co_nNi_{6-n} (0≤n≤6) Octahedral Nanoparticles

Another descriptor commonly employed to estimate the electrocatalytic activity of the nanocatalysts is the OH adsorption energy. As in the previous case of the O atom, the OH molecule was adsorbed on eight different sites for each type of nanoparticle. In Fig. 3b are illustrated the eight sites of the OH adsorption on the Pt_{44} octahedron nanoparticle. Figure 4b presents the relative OH adsorption energies on the Co_nNi_{6-n}-Pt_{38} (0≤n≤6) octahedral nanoparticles with respect to the pure Pt_{44}. It is noted that the Co_nNi_{6-n}-Pt_{38} (0≤n≤6) nanoparticles have a lower OH adsorption energy with respect to the one of pure platinum. The relative OH adsorption energy presents the same trend as the relative O adsorption energy. We notice that in general the decrease of the O and OH adsorption energies in the mixed clusters we studied is related to the increase of the number of the Ni atoms (Fig. 4).

Zhang and Henkelman found a linear relationship between the adsorption energy of the adsorbates (O, C, H, N, CO, NO, and S) and core composition of $(PdAu)_{44}$@Pt_{96} truncated octahedral nanoparticles [27]. This study found a similar dependence between the relative O and OH adsorption energies as a function of core composition of the Co_nNi_{6-n}-Pt_{38} (0≤n≤6) octahedral nanoparticles.

The relative O and OH adsorption energies values of Co_nNi_{5-n}-Pt_{38} (1≤n≤5) nanoparticles are located between the adsorption energies of the Ni_6-Pt_{38} and Co_6-Pt_{38} nanoparticles. That leads to the expectation that the Co_nNi_{5-n}-Pt_{38} (1≤n≤5) nanoparticles would present a higher electrocatalytic activity than pure Pt nanoparticles. These computational predictions were further examined by the electrochemical procedures.

Physical Characterization

Figure 5 shows the XRD patterns of $Co_{30}Ni_{70}$ milled for 30 h and $Co_{30}Ni_{70}$-20Pt/C ($Co_{30}Ni_{70}$ milled wrapped with Pt and dispersed on Vulcan carbon). The Supplementary Information Section presents the XRD patterns of $Co_{70}Ni_{30}$-20Pt/C and $Co_{70}Ni_{30}$ milled for 30 h. The XRD patterns of the precursors show an HCP structure for unmilled Co and an FCC structure for unmilled Ni, both reported in a previous study [16]. When

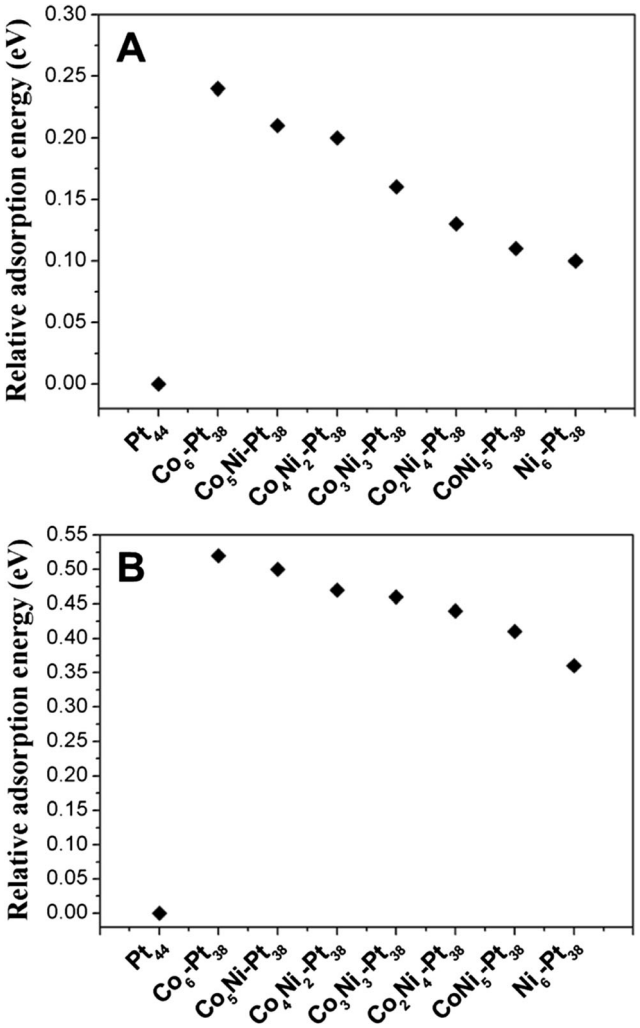

Fig. 4 Relative O and OH adsorption energies of the Co_nNi_{6-n}-Pt_{38} ($0 \le n \le 6$) nanoparticles with respect to the pure Pt_{44} system. **a** Relative O adsorption energies of the Co_nNi_{6-n}-Pt_{38} ($0 \le n \le 6$) nanoparticles with respect to the pure Pt_{44} nanoparticle. **b** Relative OH adsorption energies of the Co_nNi_{6-n}-Pt_{38} ($0 \le n \le 6$) nanoparticles with respect to the pure Pt_{44} nanoparticle

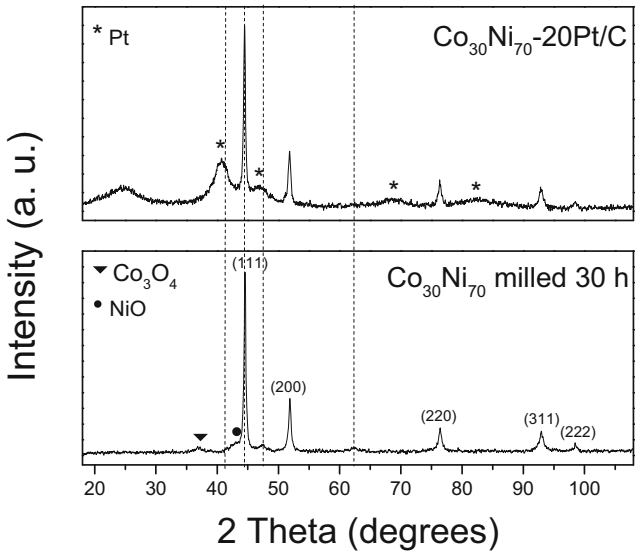

Fig. 5 XRD patterns of $Co_{30}Ni_{70}$ milled by 30 h and $Co_{30}Ni_{70}$-20Pt/C. The Miller indices on the upper diffraction pattern correspond to FCC cobalt

Co was milled separately from Ni, the starting HCP structure of Co changed completely to FCC after 30 h of milling, whereas the Ni structure did not show structure changes when it was milled separately from Co. The presence of HCP and FCC Co coexisting with FCC Ni is evidenced in Fig. 5 ($Co_{30}Ni_{70}$-20Pt/C) and in the Supplementary Information ($Co_{70}Ni_{30}$-20Pt/C), where five FCC cobalt reflections are detected (indexed planes). The dotted lines in Fig. 5 correspond to the four most intense HCP Co reflections (JCPDF 01-089-4308): (100), (002), (101), and (102). This indicates that the transformation of HCP Co to FCC Co was not completed due to the presence of Ni. The quantitative phase analysis of the $Co_{30}Ni_{70}$ system milled for 30 h indicates ~ 10 wt.% of HCP Co and ~ 90 wt.% of FCC Co, whereas that of the $Co_{70}Ni_{30}$ system milled for 30 h indicated ~ 30 wt.% of HCP Co and ~ 70 wt.% of FCC Co. The $Co_{30}Ni_{70}$ system shows two weak reflections belonging to Co_3O_4 (JCPDF 43-1003) and NiO (JCPDF 047-1049) at ~ 31.2° and ~ 43.3°, respectively.

High angle annular dark field (HAADF) images in high-resolution (HR) STEM micrograph of the mix $Co_{30}Ni_{70}$-20Pt/C are displayed in Fig. 6. The image in Fig. 6a belongs to a bright field (BF) micrograph of $Co_{30}Ni_{70}$-20Pt/C and it allows identification of the spatial distribution of the metallic particles in the carbon. Figure 6b shows bright areas corresponding to 2–5 nm crystals of size, and an auxiliary BF HRSTEM micrograph is shown in Fig. 6c. The fast Fourier transform (FFT) was obtained from the square region in Fig. 6c. FFT was used to determine the inverse fast Fourier transform (IFFT) obtained from selected reciprocal spots for image formation showing higher contrast HR images (see Fig. 6e, f). From the measured distances between the atomic planes in IFFT images, Co and Pt were identified respectively (see Fig. 6e, f). The interplanar distance observed in Co (111) is very close that of Ni (111). This result suggests that Pt coexists with Co or Ni atoms. It is worth noting that the Bragg reflection (2-theta) located at ~ 44.5° is an X-ray diffraction peak, which has contributions of Co (111) and Ni (111) overlapping each other (see Fig. 5).

Although HR-STEM has the advantage of providing specific interplanar distances for Co and Pt, a closer examination of the value obtained in Fig. 6e reveals that such interplanar distance may be attributed to either Co or Ni. Here, it is difficult to discern between Co and Ni from the interplanar distance obtained in the IFFT image in Fig. 6e since the difference between Co (111) and Ni (111) is only 0.0058 Å. Therefore, one can infer that for such IFFT image, the interplanar distance would represent either Co or Ni.

The elemental analysis of the nanoparticles was carried out by ICP-MS and EDX-SEM. EDX-SEM and ICP-MS for the

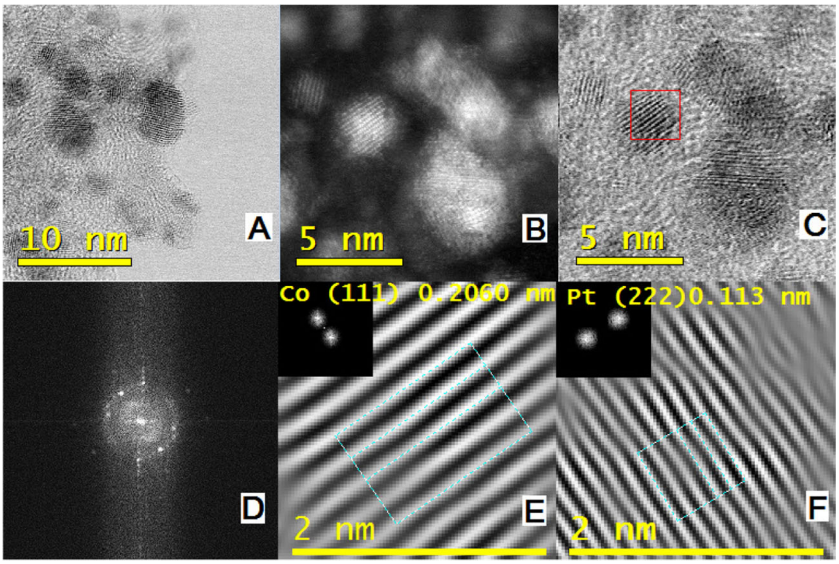

Fig. 6 TEM micrograph taken in the bright field of the overall appearance of the particles (**a**). High-resolution micrographs of dark field (**b**) and bright field (**c**); **d** corresponding fast Fourier transform of the square region in (**c**). Images (**e**) and (**f**) are the corresponding inverse fast Fourier transforms from (**d**)

$Co_{30}Ni_{70}$-20Pt/C system revealed compositions near to the nominal composition. The results obtained from EDX-SEM and ICP-MS revealed a similar composition (see Table 1). The $Co_{70}Ni_{30}$-20Pt/C sample was only measured by EDX-SEM, which also revealed a similar composition to the nominal composition (see Table 1). EDX-SEM results showed that iron contamination coming from the 30-h milling preparation in both systems $Co_{30}Ni_{70}$ and $Co_{70}Ni_{30}$ was less than 1 wt.%.

Catalytic Properties of $Co_{30}Ni_{70}$-20Pt/C and $Co_{70}Ni_{30}$-20Pt/C for the ORR

The most important electrochemical reaction for the performance of a PEM fuel cell is the ORR because of its complexity; this reaction involves multiple adsorption/desorption steps and species such as atomic oxygen (O), hydroxyl radical (OH), superoxide anion (O_2^-), and hydroperoxide anion (HO_2^-). In this reaction is desired a mechanism that involves a four-electron and four-proton pattern and avoiding as far as possible an intermediate pattern of two-electron [56–58].

Inks formed by the synthesized samples ($Co_{30}Ni_{70}$-20Pt/C and $Co_{70}Ni_{30}$-20Pt/C) were employed as electrocatalysts and working electrodes for being examined with the CV, CO stripping and RDE techniques. Figure 7a displays the CVs of the synthesized nanocatalysts contrasted with a Pt/C commercial catalyst. The CVs for both synthesized electrocatalysts show the typical profile of platinum; however, in the hydrogen zone (adsorption/desorption 0.38–0.05 V/NHE), slight differences are evident, for example, the peak centered at ~ 0.22 V/NHE of the cathodic adsorption in the commercial Pt/C does not correspond with the peak at ~ 0.29 V/NHE of the $Co_{70}Ni_{30}$-20Pt/C electrocatalyst or the peak at ~ 0.32 V/NHE of the $Co_{30}Ni_{70}$-20Pt/C electrocatalyst. For the synthesized nanocatalysts, a double-layer region is identified between ~ 0.40 and 0.7 V/RHE, whereas for the commercial Pt/C this region is shorter. Narrower peaks associated with the formation of platinum hydroxide and oxide in the anodic scan and reduction of the platinum oxides in the return sweep are detected, and the platinum oxide reduction peaks show a similar tendency in both synthesized nanocatalysts. Regarding the hydrogen adsorption/desorption peaks, a shift of 40 mV toward the anodic direction with respect to the CV of the Pt/C catalyst is also evident. In general, the CVs of the synthesized nanocatalysts agree with any typical Pt profile [59–61], and these profiles can be considered as evidence that the surface CoNi atoms were displaced by Pt atoms.

The ECSA of the $Co_{30}Ni_{70}$-20Pt/C and $Co_{70}Ni_{30}$-20Pt/C nanocatalysts was calculated using a procedure reported in the literature [62–65]. Figure 7b illustrates the peaks of CO-stripping located between + 0.6 V/NHE and + 0.8 V/NHE for the $Co_{30}Ni_{70}$-20Pt/C and $Co_{70}Ni_{30}$-20Pt/C nanocatalysts, whereas the peak of the commercial Pt/C catalyst is between + 0.7 V/NHE and + 0.9 V/NHE. The ECSA obtained from CO stripping are shown in Table 2. Particle size obtained by electrochemical measurements agrees with the particle size displayed in micrographs of Fig. 6a and b.

The CO stripping voltammograms of the $Co_{30}Ni_{70}$-20Pt/C and $Co_{70}Ni_{30}$-20Pt/C nanocatalysts presented two peaks (Fig. 7b). The $Co_{30}Ni_{70}$-20Pt/C nanocatalyst shows a peak at 0.68 V/NHE and another peak at 0.7 V/NHE. For the $Co_{70}Ni_{30}$-20Pt/C nanocatalyst, two peaks are observed as well, the first one at 0.69 V /NHE and the second one at 0.7 V/NHE. In general, any peak in these systems engages with a peak of CO oxidation of pure Pt particles. In fact, the peaks at 0.68 and 0.69 V/NHE of each system seem to be representative peaks of the CoNi system wrapped with Pt. Some researchers, for example, have explained the existence of additional peaks of CO stripping in systems with Pt nanoparticles caused by severe agglomeration [66], whereas others like Urchaga have reported overlapped peaks in CO stripping

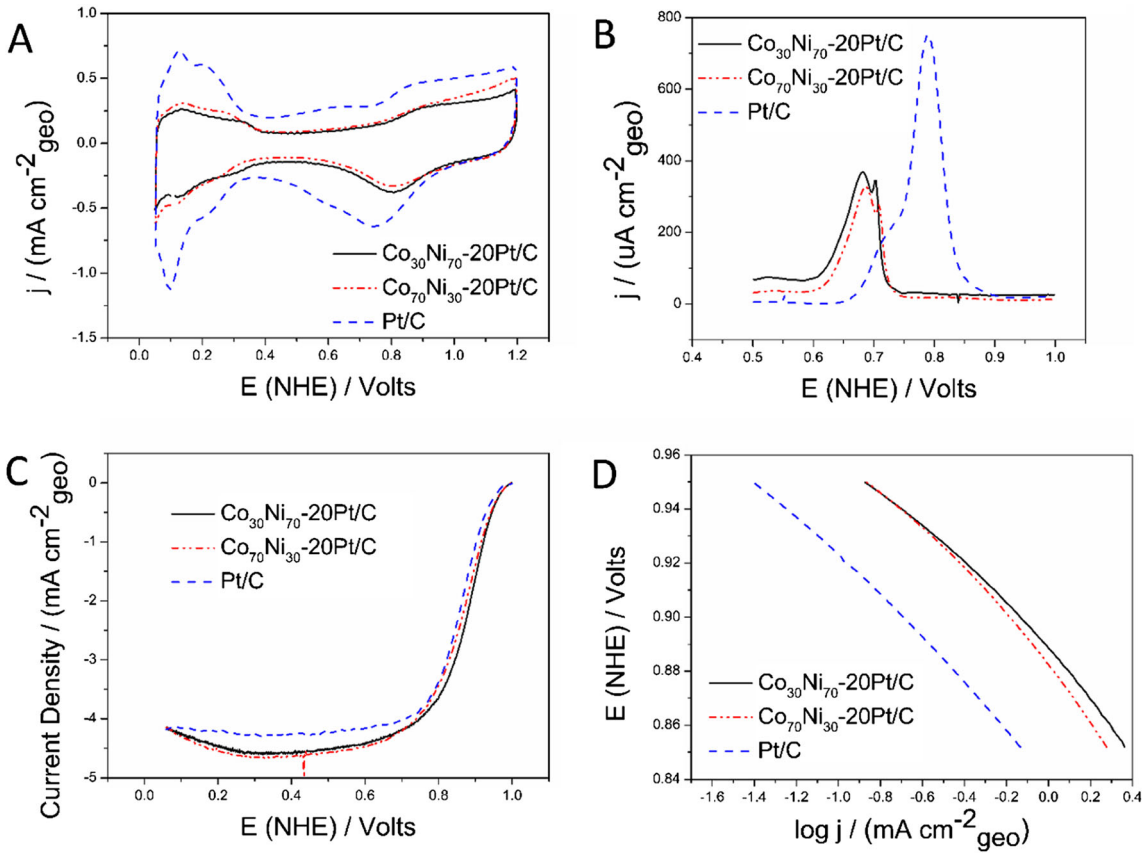

Fig. 7 Cyclic voltammograms (**a**), CO stripping (**b**), linear sweep voltammetry (**c**), and Tafel plot (**d**) of the $Co_{70}Ni_{30}$-20Pt/C, $Co_{30}Ni_{70}$-20Pt/C, and commercial Pt/C electrocatalysts

due to particles with preferential orientation such as cubic and cuboctahedral Pt particles [67]. Nevertheless, in this report, the CO peaks at 0.68 and 0.69 V/NHE could be characteristic peaks of the Pt-wrapped CoNi system because the synthesized nanocatalysts do not show any structural preferential orientation in either severe agglomeration.

The kinetics of ORR of the $Co_{30}Ni_{70}$-20Pt/C and $Co_{70}Ni_{30}$-20Pt/C nanocatalysts were analyzed by RDE because the ORR depends greatly from the hydrodynamic conditions. Figure 7c shows the *ORR polarization* curves for the $Co_{30}Ni_{70}$-20Pt/C, $Co_{70}Ni_{30}$-20Pt/C, and commercial Pt/C electrocatalysts. Kinetics control with current independent of rotation rate is observed in the range of 1.0–0.90 V/RHE. The mixed zone (kinetic/diffusion) appears between 0.90 and 0.60 V/NHE, and both synthesized nanocatalysts show a similar half-wave potential but different than the commercial Pt/C catalyst. A current density limit is observed at high overpotentials (~0.6 and 0.2 V/RHE), which is dependent on the electrode rotation speed and means that the process is controlled by the mass transport. Figure 7c displays the voltammograms of each catalyst performed at 1600 rpm; the increases in the limiting current of the synthesized nanocatalysts could be related to the increase of oxygen diffusion through the electrode surface or to the homogeneous distribution of the nanoparticles on the electrode surfaces [68].

Kinetics analyses were performed for the specific activity (SA) and the mass activity (MA) estimations. These analyses are showed in the form of the mass-transfer-corrected Tafel plots (Fig. 7d). In this work, the procedures for the kinetic current corrections and SA and MA calculations were carried

Table 2 Electrochemical active surface area (ECSA), specific activity, and mass activity of $Co_{30}Ni_{70}$-20Pt/C, $Co_{70}Ni_{30}$-20Pt/C, and Pt/C

Catalyst	Average ECSA ($m^2\ g^{-1}_{Pt}$)	Average specific activity @ 0.9 V/RHE (mA cm^{-2}_{Pt})	Std. dev. σ	Average mass activity @ 0.9 V/RHE (mA mg^{-1}_{Pt})	Std. dev. σ
$Co_{30}Ni_{70}$-20Pt/C	21.05	0.66	0.05	136.66	15.04
$Co_{70}Ni_{30}$-20Pt/C	24.91	0.55	0.04	136.33	17.78
Pt/C	49	0.19	0.007	99	10.85

out following the protocol as previously described in the literature [68]. Mean Tafel slopes are 54 mV dec^{-1} for both $Co_{30}Ni_{70}$-20Pt/C and $Co_{70}Ni_{30}$-20Pt/C. These slopes are similar to the ones obtained for Pt/C. The specific activity was normalized by ECSA whereas mass activity was with respect to the loading amount of metal Pt. The calculated SA and MA is presented in Table 2. $Co_{30}Ni_{70}$-20Pt/C and $Co_{70}Ni_{30}$-20Pt/C nanocatalysts present higher specific activities, 400% and 300%, respectively, above the value determined for Pt/C and mass activities 50% than Pt/C.

The Koutecky–Levich equation relates the current density (j) to the rotation rate (ω) of the electrode and $B = 0.2nFCD^{2/3}\upsilon^{-1/6}$ [16] where 0.2 is a constant used when ω is expressed in revolutions per minute (rpm), C is the oxygen concentration in the electrolyte (1.26×10^{-6} mol cm^{-3}), D is the oxygen diffusion coefficient in perchloric acid (1.70×10^{-5} cm^2 s^{-1}), and υ the kinematic viscosity of the perchloric acid (1.01×10^{-2} cm^2 s^{-1}) [69], and from B equation, the transferred electrons can be estimated which is $n = 3.6$ and near the multielectron $n = 4e-$ and four protons transferred for the molecular oxygen reduction for the water formation, i.e., $O_2 + 4H^+ + 4e^- \rightarrow 2H_2O$. Mean values of $B = 11.5 \times 10^{-2}$ mA cm^{-2} $rpm^{-1/2}$ were measured for both electrocatalysts and are in agreement with the 13.83×10^{-2} mA cm^{-2} $rpm^{-1/2}$ obtained for Pt/C nanoparticles, calculated under the same experimental conditions.

Conclusions

CoNi bimetallic nanoparticles wrapped with Pt were the subject of a theoretical study and experimental validation for the ORR. The theoretical study was performed to evaluate the effect of the core composition in the Pt-wrapped CoNi nanoparticles for the ORR. Pt_{44} and Co_nNi_{6-n}-Pt_{38} ($0 \leq n \leq 6$) octahedral nanoparticles were used as models and the O and OH adsorption energies were used as descriptors of the electrocatalytic activity for the ORR. This work demonstrated that the Co_nNi_{5-n}-Pt_{38} ($1 \leq n \leq 5$) nanoparticles exhibit an O and H adsorption energy weaker than the one of pure Pt, making them good candidates for the ORR. In order to corroborate the theoretical prediction on small-sized systems, CoNi bimetallic core wrapped with Pt were successively synthesized and characterized electrochemically. The experimental validation of the CoNi bimetallic nanoparticles wrapped with Pt was developed by varying the composition of the CoNi bimetallic nanoparticles ($Co_{30}Ni_{70}$-20Pt/C and $Co_{70}Ni_{30}$-20Pt/C). The presence of Ni, Co, and Pt in the synthesized nanoparticles was confirmed by EDX, XRD, and ICP-MS. The $Co_{30}Ni_{70}$-20Pt/C and $Co_{70}Ni_{30}$-20Pt/C nanocatalysts present specific activities which are three and four times higher than the commercial Pt/C, respectively. Moreover, the two novel catalysts synthesized in this study present mass activities which are 1.5 times higher than the commercial Pt/C.

Acknowledgements E. F.-R., H. C.-M., M.M. T.-C., and J.L. R.-R. acknowledge CONACYT for their doctoral fellowships. Financial support from the CONACYT projects CB-252658 and 245920 is also gratefully acknowledged. Acknowledgement is given to the Laboratorio Avanzado de Nanoscopía Electrónica from Cinvestav (Dr. Daniel Bahena Uribe for STEM micrographs and Dr. Jorge Roque Puente for the SEM analysis).

References

1. T. Jacob, The Mechanism of Forming H_2O from H_2 and O_2 over a Pt Catalyst via Direct Oxygen Reduction. Fuel Cells **6**(3-4), 159–181 (2006)
2. J. Wu, H. Yang, Platinum-Based Oxygen Reduction Electrocatalysts. Acc. Chem. Res. **46**(8), 1848–1857 (2013)
3. H. Cruz-Martínez, L. López-Sosa, O. Solorza-Feria, P. Calaminici, First-principles investigation of adsorption and dissociation of molecular oxygen on pure Pd, Ni-doped Pd and NiPd alloy clusters. Int. J. Hydrog. Energy **42**(51), 30310–30317 (2017)
4. F. Godínez-Salomón, C.P. Rhodes, K.S. Alcantara, Q. Zhu, S.E. Canton, H.A. Calderon, J.L. Reyes-Rodríguez, M.A. Leyva, O. Solorza-Feria, Tuning the oxygen reduction activity and stability of $Ni(OH)_2$@Pt/C catalysts through controlling Pt surface composition, strain, and electronic structure. Electrochim. Acta **247**, 958–969 (2017)
5. M. Shao, Q. Chang, J.P. Dodelet, R. Chenitz, Recent advances in electrocatalysts for oxygen reduction reaction. Chem. Rev. **116**(6), 3594–3657 (2016)
6. J.L. Reyes-Rodríguez, F. Godínez-Salomón, M.A. Leyva, O. Solorza-Feria, RRDE study on Co@Pt/C core–shell nanocatalysts for the oxygen reduction reaction. Int. J. Hydrog. Energy **38**(28), 12634–12639 (2013)
7. M.M. Tellez-Cruz, M.A. Padilla-Islas, J.F. Godínez-Salomón, L. Lartundo-Rojas, O. Solorza-Feria, Y-OH-decorated-Pt/C electrocatalyst for oxygen reduction reaction. Int. J. Hydrog. Energy **41**(48), 23318–23328 (2016)
8. M.T. Nguyen, R.H. Wakabayashi, M. Yang, H.D. Abruña, F.J. DiSalvo, Synthesis of carbon supported ordered tetragonal pseudo-ternary Pt 2 M′M″ (M = Fe, Co, Ni) nanoparticles and their activity for oxygen reduction reaction. J. Power Sources **280**, 459–466 (2015)
9. T. Yang, G. Cao, Q. Huang, Y. Ma, S. Wan, H. Zhao, N. Li, F. Yin, X. Sun, D. Zhang, M. Wang, Truncated octahedral platinum–nickel–iridium ternary electro-catalyst for oxygen reduction reaction. J. Power Sources **291**, 201–208 (2015)
10. M. Li, Y. Lei, N. Sheng, T. Ohtsuka, Preparation of low-platinum-content platinum–nickel, platinum–cobalt binary alloy and platinum–nickel–cobalt ternary alloy catalysts for oxygen reduction reaction in polymer electrolyte fuel cells. J. Power Sources **294**, 420–429 (2015)
11. J. Choi, Y. Lee, J. Kim, H. Lee, Enhancing stability of octahedral PtNi nanoparticles for oxygen reduction reaction by halide treatment. J. Power Sources **307**, 883–890 (2016)
12. Y. Choi, K.A. Kuttiyiel, J.P. Labis, K. Sasaki, G.G. Park, T.H. Yang, R.R. Adzic, Enhanced oxygen reduction activity of IrCu core platinum monolayer shell nano-electrocatalysts. Top. Catal. **56**(12), 1059–1064 (2013)
13. K.A. Kuttiyiel, K. Sasaki, Y. Choi, D. Su, P. Liua, R.R. Adzic, Bimetallic IrNi core platinum monolayer shell electrocatalysts for the oxygen reduction reaction. Energy Environ. Sci. **5**(1), 5297–5304 (2012)

14. K. Gong, W. Chen, K. Sasaki, D. Su, M.B. Vukmirovic, W. Zhou, E.L. Izzo, C. Perez-Acosta, P. Hirunsit, P.B. Balbuena, R.R. Adzic, Platinum-monolayer electrocatalysts: palladium interlayer on IrCo alloy core improves activity in oxygen-reduction reaction. J. Electroanal. Chem. **649**(1-2), 232–237 (2010)
15. T. Cochell, A. Manthiram, Pt@PdxCuy/C core–shell electrocatalysts for oxygen reduction reaction in fuel cells. Langmuir **28**(2), 1579–1587 (2012)
16. E. Flores-Rojas, J.G. Cabañas-Moreno, J.F. Pérez-Robles, O. Solorza-Feria, Mechanochemical synthesis of Co and Ni decorated with chemically deposited Pt as electrocatalysts for oxygen reduction reaction. Mater. Chem. Phys. **183**, 101–109 (2016)
17. E. Flores-Rojas, H. Cruz-Martínez, M.M. Tellez-Cruz, J.F. Pérez-Robles, M.A. Leyva-Ramírez, P. Calaminici, O. Solorza-Feria, Electrocatalysis of oxygen reduction on CoNi-decorated-Pt nanoparticles: a theoretical and experimental study. Int. J. Hydrog. Energy **41**(48), 23301–23311 (2016)
18. J.K. Nørskov, T. Bligaard, J. Rossmeisl, C.H. Christensen, Towards the computational design of solid catalysts. Nat. Chem. **1**(1), 37–46 (2009)
19. J.K. Nørskov, J. Rossmeisl, A. Logadottir, L. Lindqvist, Origin of the overpotential for oxygen reduction at a fuel-cell cathode. J. Phys. Chem. B **108**(46), 17886–17892 (2004)
20. V. Stamenkovic, B.S. Mun, K.J.J. Mayrhofer, P.N. Ross, N.M. Markovic, J. Rossmeisl, J. Greeley, J.K. Nørskov, Changing the activity of electrocatalysts for oxygen reduction by tuning the surface electronic structure. Angew. Chem. **118**(18), 2963–2967 (2006)
21. J. Greeley, I.E.L. Stephens, A.S. Bondarenko, T.P. Johansson, H.A. Hansen, T.F. Jaramillo, J. Rossmeisl, I. Chorkendorff, J.K. Nørskov, Alloys of platinum and early transition metals as oxygen reduction electrocatalysts. Nat. Chem. **1**(7), 552–556 (2009)
22. H.C. Tsai, T.H. Yu, Y. Sha, B.V. Merinov, P.W. Wu, S.Y. Chen, W.A. Goddard III, Density functional theory study of Pt3M alloy surface segregation with adsorbed O/OH and Pt3Os as catalysts for oxygen reduction reaction. J. Phys. Chem. C **118**(46), 26703–26712 (2014)
23. R. Callejas-Tovar, P.B. Balbuena, Effect of subsurface vacancies on oxygen reduction reaction activity of Pt-based alloys. J. Phys. Chem. C **116**(27), 14414–14422 (2012)
24. B.B. Xiao, X.B. Jiang, Q. Jiang, Density functional theory study of oxygen reduction reaction on Pt/Pd3Al(111) alloy electrocatalyst. Phys. Chem. Chem. Phys. **18**(21), 14234–14243 (2016)
25. P.C. Jennings, H.A. Aleksandrov, K.M. Neyman, R.L. Johnston, A DFT study of oxygen dissociation on platinum based nanoparticles. Nanoscale **6**(2), 1153–1165 (2014)
26. S. Praserthdam P.B. Balbuena, Effects of oxygen coverage, catalyst size, and core composition on Pt-alloy core-shell nanoparticles for oxygen reduction reaction. Catal. Sci. Technol. **6**(13), 5168–5177 (2016)
27. L. Zhang, G. Henkelman, Computational Design of Alloy-Core@Shell Metal Nanoparticle Catalysts. ACS Catal. **5**(2), 655-660 (2015)
28. R.M. Anderson, D.F. Yancey, L. Zhang, S.T. Chill, G. Henkelman, R.M. Crooks, A theoretical and experimental approach for correlating nanoparticle structure and electrocatalytic activity. Acc. Chem. Res. **48**(5), 1351–1357 (2015)
29. G. Ramos-Sanchez, S. Praserthdam, F. Godinez-Salomon, C. Barker, M. Moerbe, H.A. Calderon, L.A. Lartundo, M.A. Leyva, O. Solorza-Feria, P.B. Balbuena, Challenges of modelling real nanoparticles: Ni@Pt electrocatalysts for the oxygen reduction reaction. Phys. Chem. Chem. Phys. **17**(42), 28286–28297 (2015)
30. H.C. Tsai, Y.C. Hsieh, T.H. Yu, Y.J. Lee, Y.H. Wu, B.V. Merinov, P.W. Wu, S.Y. Chen, R.R. Adzic, W.A. Goddard III, DFT study of oxygen reduction reaction on Os/Pt core–shell catalysts validated by electrochemical experiment. ACS Catal. **5**(3), 1568–1580 (2015)
31. L. Zhang, R. Iyyamperumal, D.F, Yancey, R.M. Crooks, G. Henkelman, Design of Pt-Shell Nanoparticles with Alloy Cores for the Oxygen Reduction Reaction. ACS nano **7**(10), 9168–9172 (2013)
32. S.P. Lin, K.W. Wang, C.W. Liu, H.S. Chen, J.H. Wang, Trends of oxygen reduction reaction on platinum alloys: a computational and experimental study. J. Phys. Chem. C **119**(27), 15224–15231 (2015)
33. G. Geudtner, P. Calaminici, J. Carmona-Espíndola, J.M. del Campo, V.D. Domínguez-Soria, R.F. Moreno, G.U. Gamboa, A. Goursot, A.M. Köster, J.U. Reveles, T. Mineva, J.M. Vásquez-Pérez, A. Vela, B. Zúñiga-Gutierrez, D.R. Salahub, deMon2k. Wiley Interdiscip. Rev. Comput. Mol. Sci. **2**(4), 548–555 (2012)
34. A.M. Koster, G. Geudtner, A. Alvarez-Ibarra, P. Calaminici, M.E. Casida, J. Carmona-Espindola, V.D. Dominguez, R. Flores-Moreno, G.U. Gamboa, A. Goursot, T. Heine, A. Ipatov, A. de la Lande, F. Janetzko, J.M. del Campo, D. Mejia-Rodriguez, J.U. Reveles, J. Vasquez-Perez, A. Vela, B. Zuniga-Gutierrez, D.R. Salahub, *deMon2k, version*, vol 4 (The deMon developers, Cinvestav, Mexico City, 2016)
35. V.I. Lebedev, A quadrature formula for the sphere of 59th algebraic order of accuracy. Russian Acad. Sci. Dokl. Math. **50**(2), 283–286 (1995)
36. P.M.W. Gill, B.G. Johnson, J.A. Pople, A standard grid for density functional calculations. Chem. Phys. Lett. **209**(5-6), 506–512 (1993)
37. B.I. Dunlap J.W.D. Connolly, J.R. Sabin, On first-row diatomic molecules and local density models. J. Chem. Phys. **71**(12), 4993–4999 (1979)
38. J.W. Mintmire, B.I. Dunlap, Fitting the Coulomb potential variationally in linear-combination-of-atomic-orbitals density-functional calculations. Phys. Rev. A **25**(1), 88–95 (1982)
39. Y. Zhang, W. Yang, Comment on "Generalized gradient approximation made simple". Phys. Rev. Lett. **80**(4), 890 (1998)
40. J.P. Perdew, K. Burke, M. Ernzerhof, Generalized gradient approximation made simple. Phys. Rev. Lett. **77**(18), 3865–3868 (1996)
41. K.L. Schuchardt, B.T. Didier, T. Elsethagen, L. Sun, V. Gurumoorthi, J. Chase, J. Li, T.L. Windus, Basis set exchange: a community database for computational sciences. J. Chem. Inf. Model. **47**(3), 1045–1052 (2007)
42. P. Calaminici, F. Janetzko, A.M. Köster, R. Mejia-Olvera, B. Zuniga-Gutierrez, Density functional theory optimized basis sets for gradient corrected functionals: 3d transition metal systems. J. Chem. Phys. **126**(4), 44108 (2007)
43. A.M. Köster, J.U. Reveles, J.M. del Campo, Calculation of exchange-correlation potentials with auxiliary function densities. J. Chem. Phys. **121**(8), 3417–3424 (2004)
44. J.U. Reveles, A.M. Köster, Geometry optimization in density functional methods. J. Comput. Chem. **25**(9), 1109–1116 (2004)
45. A. Ezeta, E.M. Arce, O, Solorza, R.G. González, H. Dorantes, Effect of the leaching of Ru-Se-Fe and Ru-Mo-Fe obtained by mechanical alloying on electrocatalytical behavior for the oxygen reduction reaction. J. Alloys Compd. **483**(1-2), 429–431 (2009)
46. P. Sotelo-Mazón, R.G. González-Huerta, J.G. Cabañas-Moreno, O. Solorza-Feria, Mechanically milled Ru_xFe_y electrocatalyst for oxygen reduction in acid media. Int. J. Electrochem. **2**(7), 523–533 (2007)
47. M.A. García-Contreras, S.M. Fernández-Valverde, J.R. Vargas-García, M.A. Cortés-Jácome, J.A. Toledo-Antonio, C. Angeles-Chavez, Pt, PtCo and PtNi electrocatalysts prepared by mechanical alloying for the oxygen reduction reaction in 0.5M H2SO4. Int. J. Hydrog. Energy **33**(22), 6672–6680 (2008)
48. C.A. Cortes-Escobedo, R.G. Gonzalez-Huerta, A.M. Bolarín-Miró, F.S. de Jesús, Q. Zhu, S.E. Canton, K. Suarez-Alcantara, M. Tufiño-Velazquez, Mechanically activated Pt–Ni and Pt–Co alloys as electrocatalysts in the oxygen reduction reaction. Int. J. Hydrog. Energy **39**(29), 16722–16730 (2014)
49. Q. Jia, W. Liang, M.K. Bates, P. Mani, W. Lee, S. Mukerjee, Activity descriptor identification for oxygen reduction on platinum-based bimetallic nanoparticles: in situ observation of the

linear composition–strain–activity relationship. ACS Nano **9**(1), 387–400 (2015)
50. I.E.L. Stephens, A.S. Bondarenko, U. Gronbjerg, J. Rossmeisl, I. Chorkendorff, Understanding the electrocatalysis of oxygen reduction on platinum and its alloys. Environ. Sci. **5**(5), 6744–6762 (2012)
51. A.J. Medford, A. Vojvodic, J.S. Hummelshøj, J. Voss, F. Abild-Pedersen, F. Studt, T. Bligaard, A. Nilsson, J.K. Nørskov, From the Sabatier principle to a predictive theory of transition-metal heterogeneous catalysis. J. Cat. **328**, 36–42 (2015)
52. C. di Paola, F. Baletto, Oxygen adsorption on small PtNi nanoalloys. Phys. Chem. Chem. Phys. **13**(17), 7701–7707 (2011)
53. J. Shin, J.H. Choi, P.R. Cha, S.K. Kim, I. Kim, S.C. Lee, D.S. Jeong, Catalytic activity for oxygen reduction reaction on platinum-based core-shell nanoparticles: all-electron density functional theory. Nanoscale **7**(38), 15830–15839 (2015)
54. J. Zhang, H. Yang, J. Fang, S. Zou, Synthesis and oxygen reduction activity of shape-controlled Pt3Ni nanopolyhedra. Nano Lett. **10**(2), 638–644 (2010)
55. C. Cui, L. Gan, M. Heggen, S. Rudi, P. Strasser, Compositional segregation in shaped Pt alloy nanoparticles and their structural behaviour during electrocatalysis. Nat. Mater. **12**(8), 765–771 (2013)
56. W.T. Hong, M. Risch, K.A. Stoerzinger, A. Grimaud, J. Suntivich, Y. Shao-Horn, Toward the rational design of non-precious transition metal oxides for oxygen electrocatalysis. Energy Environ. Sci. **8**(5), 1404–1427 (2015)
57. F. Cheng, J. Chen, Metal-air batteries: from oxygen reduction electrochemistry to cathode catalysts. Chem. Soc. Rev. **41**(6), 2172-2192 (2012)
58. R.R. Adzic, Platinum monolayer electrocatalysts: tunable activity, stability, and self-healing properties. Electrocatalysis **3**(3–4), 163–169 (2012)
59. K.J.J. Mayrhofer, V. Juhart, K. Hartl, M. Hanzlik, M. Arenz, Adsorbate-Induced Surface Segregation for Core–Shell Nanocatalysts. Angew. Chem. Int. **48**(19), 3529-3531 (2009)
60. Y. Nie, L. Li, W. Wei, Recent advancements in Pt and Pt-free catalysts for oxygen reduction reaction. Chem. Soc. Rev. **44**(8), 2168–2201 (2015)
61. Y.J. Wang, N. Zhao, B. Fang, H. Li, X.T. Bi, H. Wang, Carbon-supported Pt-based alloy electrocatalysts for the oxygen reduction reaction in polymer electrolyte membrane fuel cells: particle size, shape, and composition manipulation and their impact to activity. Chem. Rev. **115**(9), 3433–3467 (2015)
62. T. Vidakovic, M. Christov, K. Sundmacher, The use of CO stripping for in situ fuel cell catalyst characterization. Electrochim. Acta **52**(18), 5606–5613 (2007)
63. D. Chen, Q. Tao, L. Wen Liao, S. Xiong Liu, Y. Xia Chen, Determining the active surface area for various platinum electrodes. S.Ye, Electrocatal. **2**(3), 207–219 (2011)
64. K.J.J. Maryhofer, M. Arenz, B.B. Blizanac, V. Stamenkovic, P.N. Ross, N.M. Markovic, CO surface electrochemistry on Pt-nanoparticles: a selective review. Electrochim. Acta **50**(25–26), 5144–5154 (2005)
65. F. Maillard, E.R. Svinova, U. Stimming, CO monolayer oxidation on Pt nanoparticles: further insights into the particle size effects. J. Electroanal. Chem. **599**(2), 221–232 (2007)
66. F. Maillard, S. Schreier, M. Hanzlik, E.R. Savinova, S. Weinkaul, U. Stimming, Influence of particle agglomeration on the catalytic activity of carbon-supported Pt nanoparticles in CO monolayer oxidation. Phys. Chem. Chem. Phys. **7**(2), 385–393 (2005)
67. P. Urchaga, S. Baranton, C. Coutanceau, G. Jerkiewicz, Electrooxidation of COchemon Pt nanosurfaces: solution of the peak multiplicity puzzle. Langmuir **28**(7), 3658–3663 (2012)
68. Y. Garsany, O.A. Baturina, K.E. Swider-Lyons, S.S. Kocha, Experimental methods for quantifying the activity of platinum electrocatalysts for the oxygen reduction reaction. Anal. Chem. **82**(15), 6321–6328 (2010)
69. S. Beyhan, N.E. Şahin, S. Pronier, J.M. Léger, F. Kadırgan, Comparison of oxygen reduction reaction on Pt/C, Pt-Sn/C, Pt-Ni/C, and Pt-Sn-Ni/C catalysts prepared by Bönnemann method: a rotating ring disk electrode study. Electrochim. Acta **151**, 565–573 (2015)